INTERNATIONAL JOURNAL FOR NUMERICAL METHODS IN FLUIDS, VOL. 5, 685–707 (1985)

CONFORMING FINITE ELEMENT COMPUTATIONS APPLIED TO A SPATIALLY PERIODIC, HARMONIC NAVIER–STOKES PROBLEM

LIONEL BORNE

Ecole Nationale des Travaux Publics de l'Etat, Rue Maurice Audin, 69120 Vaulx-en-Velin, France

AND

RENÉ CHAMBON AND JEAN-LOUIS AURIAULT

Institut de Mécanique de Grenoble, B. P. 68, 38402 Saint-Martin-d'Heres Cedex, France

SUMMARY

In this paper computations in the two dimensional case of a harmonic Navier–Stokes problem with periodic boundary conditions are presented. This study of an incompressible viscous fluid leads to a non-symmetric linear problem (very low Reynolds number). Moreover unknown functions have complex values (monochromatic dynamic behaviour). Numerical treatment of the incompressibility condition is a generalization of the classical treatment of Stokes problem. A mixed formulation, where discrete pressure plays the role of Lagrange multipliers is used (Uzawa algorithm).

Two conforming finite element methods are tested on different meshes. The second one uses a classical refinement in the shape function: the so-called bulb function. All computational tests show that the use of a bulb function on each element gives better results than refinement in the mesh without introducing too many degrees of freedom. Finally numerical results are compared to experimental data.

KEY WORDS Navier–Stokes Problem Monochromatic Dynamic Behaviour Uzawa Algorithm Darcy's Law Conforming Finite Element Methods

INTRODUCTION

This work is a numerical checking of the generalized Darcy's law. This law is the generalization for dynamic filtration through saturated porous media of the classical Darcy's law. It was theoretically studied by Auriault.[1]

First the main assumptions and results are recalled. Further details are available in References 1–5. Let us underline here one fundamental assumption: the spatial periodicity of the whole problem. If one period is called Ω then this assumption would be denoted as the Ω-periodicity condition.

A second part deals with the two discrete problems which are used for numerical computations. The existence and uniqueness theorems and the convergence of the discrete solution are not established in this particular case. All these results are given in References 6 and 7 for the case of real unknown functions (Stokes problem). The convergence of the algorithm used here is demonstrated.

Then the implementation of these two approximations is explained and several tests are

0271–2091/85/080685–23$02.30 *Received March 1984*

performed. In particular the convergence of the Uzawa algorithm for increasing frequencies is tested.

Finally computations of an example are presented and compared with experimental results.

GENERALIZED DARCY'S LAW—PROBLEM TO BE SOLVED

Assumptions and notations

Assumptions. In the following, only two dimensional, periodic problem are treated. Two periods Ω are sketched in Figure 1. The whole geometrical problem is given when the period Ω is known. All unknown functions are considered as spatially periodic. This property is called Ω-periodicity. For instance, for the case of Figure 1, it means:

$$\forall m, n \in \mathbb{N}, \quad F(x_1 + np_1, x_2 + mp_2, \ldots) = F(x_1, x_2, \ldots)$$

Let us note that the generalized law of Darcy is built into the general (three dimensional case). The present numerical study is restricted to the two dimensional case to simplify the implementation and reduce computation time.

The fluid is assumed to be viscous Newtonian and incompressible. The velocity field is small enough to satisfy linearized Navier–Stokes equations. This means that the convective terms are negligible (very low Reynolds number for the flow), on the other hand the linear dynamical terms are taken into account.

Notations.

ρ fluid mass per unit of volume

μ dynamic viscosity

v_j velocity field components, the unknown periodic functions

p unknown pressure, also Ω-periodic

x_j spatial variables

t time variable

F_j 'body force' components. This force generates the flow through the porous saturated media. Let us call the scale of one period, the microscopic scale. The scale of a large number of periods is the macroscopic scale. At the time t, the components F_j are constant on the

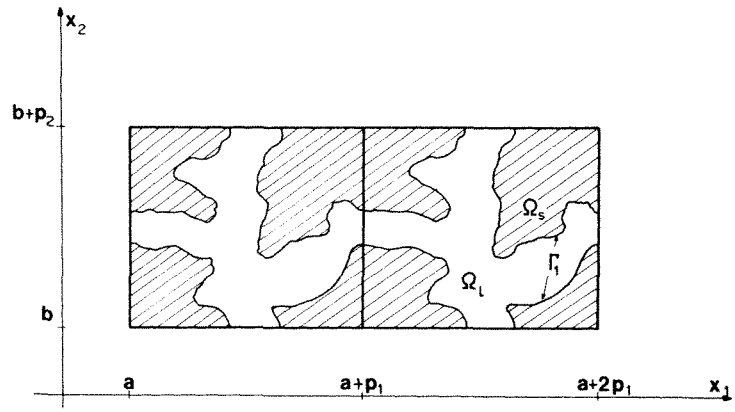

Figure 1. Two periods Ω of a porous media; Ω_l = fluid domain; Ω_s = solid domain; Γ_1 = fluid–solid interface

period. F_j describes the macroscopic pressure gradient. p is then a fine description of the pressure distribution on a period.[4]

Under these assumptions and notations, the equations governing the problem can be written (on the microscopic scale):

$$\mu \frac{\partial^2 v_j}{\partial x_k \partial x_k} + \frac{\partial p}{\partial x_j} + F_j = \rho \frac{\partial v_j}{\partial t}, \tag{1}$$

$$\frac{\partial v_j}{\partial x_j} = 0 \quad \text{(incompressibility condition)}. \tag{2}$$

Then if the problem is studied under constant frequency (harmonic study), the unknown functions v_j and p and the 'body force' components can be written in the form

$$v_j = \hat{v}_j e^{i\omega t},$$
$$p = \hat{p} e^{i\omega t},$$
$$F_j = \hat{F}_j e^{i\omega t},$$

where ω is a constant pulsation, and $\hat{v}_j$, $\hat{p}$, $\hat{F}_j$ are complex numbers without time dependence.

By substitution and eliminating $e^{i\omega t}$ in (1) and (2) they become

$$\mu \frac{\partial^2 \hat{v}_j}{\partial x_k \partial x_k} + \frac{\partial \hat{p}}{\partial x_j} + F_j = i\omega\rho \hat{v}_j, \tag{3}$$

$$\frac{\partial \hat{v}_j}{\partial x_j} = 0. \tag{4}$$

In the following, the complex numbers $\hat{v}_j$, $\hat{p}$, $\hat{F}_j$ can be denoted by v_j, p, F_j without any possible confusion. To simplify, the static parts of the quantities v_j, p, F_j have been taken equal to zero. Static contributions could be added to these quantities without changing equations (3) and (4). Then harmonic flow would be superposed on a permanent flow.

In order to solve the problem (3), (4), it is necessary to add boundary conditions.

Problem to be solved

Let us denote by $\Gamma_2 = \partial\Omega_l - \Gamma_1$, where $\partial\Omega_l$ is the boundary of the fluid domain and Γ_1 is the fluid–solid interface.

The unknown complex functions v_j and p would be defined on Ω_l, and the components F_j are complex constants on Ω_l. Then v_j and p are solutions of

$$\forall M \in \Omega_l \begin{cases} \mu \dfrac{\partial^2 v_j}{\partial x_k \partial x_k} + \dfrac{\partial p}{\partial x_j} + F_j = i\omega\rho v_j, \\ \dfrac{\partial v_j}{\partial x_j} = 0, \\ v_j = 0 \quad \text{on } \Gamma_1 \text{ and } v_j, p \ \Omega\text{-periodic on } \Gamma_2. \end{cases} \tag{5}$$

Let us note some particular points of this linear Navier–Stokes problem:

(a) The unknown functions are complex.

(b) The boundary conditions are not homogeneous on $\partial\Omega_l$ but only on Γ_1. On $\partial\Omega_l - \Gamma_1 = \Gamma_2$ the boundary conditions are the Ω-periodicity conditions.

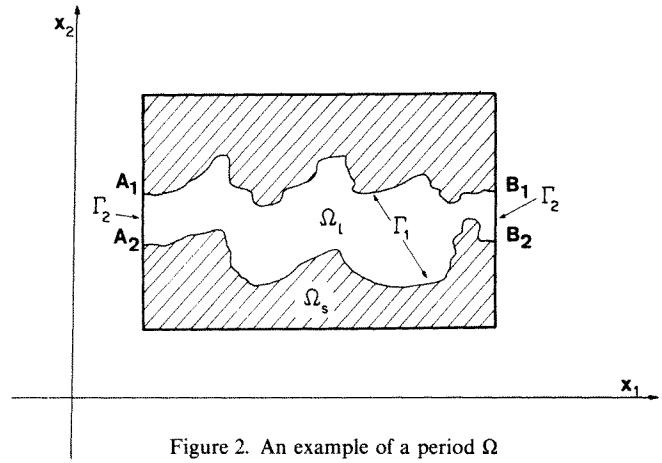

Figure 2. An example of a period Ω

For instance, for the geometry of Figure 2, it means the same pressure distribution and velocity field on the segments $\overline{A_1A_2}$ and $\overline{B_1B_2}$.

(c) And, finally, the incompressibility condition must be satisfied, but with complex unknown functions (an extension of the classical difficulty).

Solution of problem (5)

Existence and uniqueness results for the solution of this linear problem are available in References 1–3. It is shown that the unique solution can be written as

$$\forall M \in \Omega_l, \quad v_j(M) = k_{jl}(\omega, M) F_l. \tag{6}$$

On the macroscopic scale, the physical quantity which is significant is the flow of fluid through the porous media. Since F_l is constant on Ω_l,

$$\frac{1}{|\Omega|} \int_{\Omega_l} v_j \mathrm{d}\Omega = K_{jl}(\omega) F_l, \tag{7}$$

with

$$K_{jl}(\omega) = \frac{1}{|\Omega|} \int_{\Omega_l} k_{jl}(\omega, M) \mathrm{d}\Omega. \tag{8}$$

$K_{jl}(\omega)$ are complex components of a macroscopic second order tensor $K(\omega)$. As for the classical law of Darcy, $\mathbf{K}(\omega)$ is a permeability tensor, symmetric and reversible. Notice that the inverse tensor $\mathbf{H}(\omega) = \mathbf{K}^{-1}(\omega)$ has a clear physical meaning:

$$\mathbf{H}(\omega) = \mathbf{H1}(\omega) + \mathrm{i}\mathbf{H2}(\omega).$$

The second order tensors $\mathbf{H1}(\omega)$ and $\mathbf{H2}(\omega)$ have real components which are, respectively, the real part and imaginary parts of the complex components of $\mathbf{H}(\omega)$. $\mathbf{H1}(\omega)$ is representative of the viscous dissipation and $\mathbf{H2}(\omega)$ is an inertial term.[4,5]

NUMERICAL PROBLEM

For the geometrical case of Figure 3, it is obvious that Ox_1, Ox_2, Ox_3 are the eigendirections for the tensor $\mathbf{K}(\omega)$. The components of $\mathbf{K}(\omega)$ in x_1, x_2, x_3 axes should be represented by the

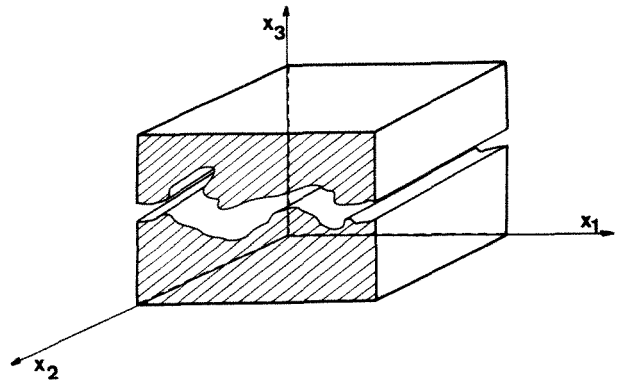

Figure 3. A typical period for our study

following matrix:

$$\begin{bmatrix} K_{11}(\omega) & 0 & 0 \\ 0 & K_{22}(\omega) & 0 \\ 0 & 0 & 0 \end{bmatrix}_{(x_1,x_2,x_3)}.$$

If the 'body force' **F** is in the x_1 direction, the study of the flow will give only the component $K_{11}(\omega)$. It is the aim of this study.

Finally, the numerical problem to solve is the problem (5) in fluid domain Ω_l as shown in Figure 2 for body forces in the x_1 direction.

Weak formulation

Let us define E as:

$$E = \left\{ \begin{array}{l} \mathbf{v} = \begin{pmatrix} v_1 \\ v_2 \end{pmatrix}, v_j (j = 1, 2) \text{ complex functions defined } \forall M \in \Omega_l \\ \text{and so that } \dfrac{\partial v_j}{\partial x_j} = 0; v_j \ \Omega\text{-periodic}; v_j = 0 \text{ on } \Gamma_1 \end{array} \right\}.$$

To find v_j and p which are a solution of (5) is equivalent to finding $\mathbf{v} \in E$ so that $\forall \boldsymbol{\alpha} \in E$

$$\mu \int_{\Omega_l} \frac{\partial v_j}{\partial x_l} \frac{\partial \bar{\alpha}_j}{\partial x_l} \mathrm{d}\Omega + \mathrm{i}\omega\rho \int_{\Omega_l} v_j \bar{\alpha}_j \mathrm{d}\Omega = \int_{\Omega_l} F_j \bar{\alpha}_j \mathrm{d}\Omega. \tag{9}$$

($\bar{\alpha}_j$ represents the conjugate complex number of α_j).

The existence and uniqueness of the solution $\mathbf{v} \in E$ for this weak formulation are obtained by application of the Lax–Milgram theorem.[1,3]

Another weak formulation is possible on the space F defined by

$$F = \left\{ \begin{array}{l} \mathbf{v} = \begin{pmatrix} v_1 \\ v_2 \end{pmatrix}, \quad v_j (j = 1, 2) \text{ complex functions defined } \forall M \in \Omega_l \\ \text{and so that } v_j \text{ is } \Omega\text{-periodic on } \Gamma_2, v_j = 0 \text{ on } \Gamma_1 \end{array} \right\}.$$

Let us define the space

$$G = \{p, \text{ complex function defined } \forall M \in \Omega_l, \ \Omega\text{-periodic on } \Gamma_2\}.$$

Then the weak formulation on F can be written:

To find $\mathbf{v}\in F$, $p\in G$ so that, $\forall \boldsymbol{\alpha}\in F$,

$$\mu\int_{\Omega_l}\frac{\partial v_j}{\partial x_l}\frac{\partial \bar{\alpha}_j}{\partial x_l}\mathrm{d}\Omega+\mathrm{i}\omega\rho\int_{\Omega_l}v_j\bar{\alpha}_j\mathrm{d}\Omega+\int_{\Omega_l}p\frac{\partial\bar{\alpha}_j}{\partial x_j}\mathrm{d}\Omega=\int_{\Omega_l}F_j\bar{\alpha}_j\mathrm{d}\Omega \tag{10}$$

and

$$\operatorname{div}\mathbf{v}=0.$$

In the following, only this second formulation is used. To solve numerically the problem (5) by the finite element method means to build a discrete problem on a finite dimensional space ('numerical space'). Then the numerical solution is built on a basis of the numerical space.

Elements well-adapted to the incompressibility condition are complex to build and the use of such elements is restrictive. Then a discrete problem for the formulation on the space E is difficult to build.

It is more easy to build a discrete problem for the formulation on F. Then the incompressibility condition is not satisfied at each point of Ω_l. Only the following relation is checked:

$$\int_{\varphi_e}q\frac{\partial v_j}{\partial x_j}\mathrm{d}\Omega=0,$$

where

φ_e is any finite element of the discretization

q is a linear function to be precised.

To satisfy this average condition the Uzawa algorithm is used. The unknown discrete functions v_j are continuous from one element to another.

Two conforming finite element methods are used. These methods are extension for complex unknown functions of the ones presented by Crouzeix and Raviart[8] for solving the stationary Stokes equations ($\omega=0$).

First discrete problem

Let us define a discretization by a set of T triangles. Each triangle is denoted by $\varphi_e, \forall e\in\{1,2,\ldots,T\}$. Ω_l^{d} is defined by: $\Omega_l^{\mathrm{d}}=\bigcup_{e=1}^{T}\varphi_e$.

On each element, the velocity component v_j^e is defined by the classical quadratic interpolation. Barycentric co-ordinates L_1, L_2, L_3 are used in the following with $L_1+L_2+L_3=1$.

At each point M of a triangular element φ_e, v_j^e is given by

$$\forall M\in\varphi_e;\quad v_j^e(M)=\sum_{k=1}^{6}v_j(M_k)\phi_k^e(M),$$

where

$$\phi_k^e(M)=L_k(2L_k-1);\quad k=1,2,3,$$
$$\phi_4^e(M)=4L_1L_2,$$
$$\phi_5^e(M)=4L_2L_3,$$
$$\phi_6^e(M)=4L_1L_3,$$

are the shape functions and $v_j(M_k)$ the nodal unknown components of the complex velocity of the node (see Figure 4).

The six nodes on each triangle are the three vertices of the element and the mid-point of each side.

Let us note that if the discrete velocity is continuous from one element to another the discrete

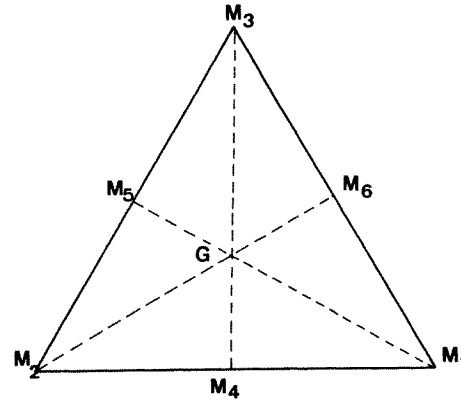

Figure 4. One finite element φ_e

pressure is discontinuous. On one element the complex pressure $p^e(M)$ is constant. The incompressibility condition is partially satisfied on each triangle φ_e by

$$\int_{\varphi_e} \frac{\partial v_j}{\partial x_j} \mathrm{d}\Omega = 0.$$

W will denote the discrete space of functions, the restrictions of which on any triangle φ_e are defined by the previous formulae.

The discrete pressure p^d on Ω_l^d, is defined as a constant value on each triangular element. It is discontinuous from one element to another. Q will denote the discrete space of these pressures. Both spaces Q and W obviously have finite dimensions.

But to refine this numerical model, as is shown in Reference 8 by Crouzeix and Raviart for the Stokes problem, a second discrete problem is presented.

Second discrete problem

In this case, on each element φ_e, v_j^e is defined by

$$\forall M \in \varphi_e, \quad v_j^e(M) = v_j'^e(M) + L_1 L_2 L_3 B_j,$$

where

$L_1 L_2 L_3$ is the so-called bulb function
$v_j'^e(M)$ is the quadratic interpolation of the previous subsection.
B_j is an unknown vector component, like the previous nodal unknown $v_j(M_i)$

Now each element presents seven nodes: the six previous nodes and the barycentre **G** of the element.

The unknown pressure is defined on each element φ_e by a linear function:

$$\forall M \in \varphi_e; \quad p^e(M) = \sum_{i=1}^{3} L_i p(M_i).$$

Let us note that the discrete velocity is always continuous. The incompressibility condition is better satisfied but always partially by

$$\forall e = 1, 2, \ldots, T; \quad \int_{\varphi_e} \frac{\partial v_j}{\partial x_j} \mathrm{d}\Omega = 0 \quad \text{and} \quad \int_{\varphi_e} x_k \frac{\partial v_j}{\partial x_j} \mathrm{d}\Omega = 0 \quad (k = 1, 2).$$

The discrete pressure is always discontinuous from one element to another. In the same manner

as in the previous subsection, $\tilde{W}$ and $\tilde{Q}$ are the associated discrete spaces for velocity and pressure unknowns. Then the discrete problem can be written:

Find $\mathbf{v} \in W$ (resp $\tilde{W}$) and $p \in Q$ (resp $\tilde{Q}$) such that $\forall \boldsymbol{\alpha} \in W(\tilde{W})$

$$\mu \int_{\Omega_l^d} \frac{\partial v_j}{\partial x_k} \frac{\partial \bar{\alpha}_j}{\partial x_k} d\Omega + i\omega\rho \int_{\Omega_l^d} v_j \bar{\alpha}_j d\Omega + \int_{\Omega_l^d} p \frac{\partial \bar{\alpha}_j}{\partial x_j} d\Omega = \int_{\Omega_l^d} F_j \bar{\alpha}_j d\Omega \tag{11}$$

and

$$\frac{\partial v_j}{\partial x_j} = 0. \tag{12}$$

(11) leads to a linear system to be solved if the discrete pressure is known. Then to satisfy partially (12) and obtain the discrete pressure p, the Uzawa algorithm is used.

Numerical algorithm: Uzawa algorithm (see Reference 7 for the Stokes problem)

Let us define some notations:

$$((\mathbf{v}, \boldsymbol{\alpha})) = \int_{\Omega_l^d} \frac{\partial v_j}{\partial x_l} \frac{\partial \bar{\alpha}_j}{\partial x_l} d\Omega; \quad \|\mathbf{v}\|^2 = ((\mathbf{v}, \mathbf{v})),$$

$$(\mathbf{v}, \boldsymbol{\alpha}) = \int_{\Omega_l^d} v_j \bar{\alpha}_j d\Omega; \quad |\mathbf{v}|^2 = (\mathbf{v}, \mathbf{v}),$$

$$(p, q) = \int_{\Omega_l^d} p \bar{q} d\Omega; \quad |p|^2 = (p, p),$$

and $|q|_C$ is the modulus of the complex number q.

Then, with these notations (11) becomes

$$\mu((\mathbf{v}, \boldsymbol{\alpha})) + i\omega\rho(\mathbf{v}, \boldsymbol{\alpha}) + (p, \operatorname{div} \boldsymbol{\alpha}) = (\mathbf{F}, \boldsymbol{\alpha}). \tag{13}$$

In the following the superscript in parentheses indicates the step of the algorithm. If the pressure values at step m are given, the unknown velocity at step $m+1$ is computed by: $\forall \boldsymbol{\alpha} \in W(\tilde{W}), \mathbf{v}^{(m+1)} \in W(\tilde{W})$

$$\mu((\mathbf{v}^{(m+1)}, \boldsymbol{\alpha})) + i\omega\rho(\mathbf{v}^{(m+1)}, \boldsymbol{\alpha}) = (\mathbf{F}, \boldsymbol{\alpha}) - (p^{(m)}, \operatorname{div} \boldsymbol{\alpha}). \tag{14}$$

Then the unknown pressure is computed by $p^{(m+1)} \in Q(\tilde{Q})$; $\forall q \in Q(\tilde{Q})$

$$(p^{(m+1)} - p^{(m)}, q) - C(\operatorname{div} \mathbf{v}^{(m+1)}, q) = 0, \tag{15}$$

where C is a constant to be defined, to obtain faster convergence of the algorithm.

The first step of the algorithm is to assume initial pressure $p^{(0)}$

Study of the convergence of the Uzawa algorithm. We present in the following an extension to complex unknown functions of the classical proof of convergence of the Uzawa algorithm (see for instance Reference 7).

If v and p denote the discrete solution on W and Q (respectively $\tilde{W}$ and $\tilde{Q}$) of the problem, $\forall \boldsymbol{\alpha} \in W(\tilde{W})$, $\mathbf{v}$ and p satisfy (13).

If $\mathbf{v}^{(m+1)}$ is the solution of (14), as $\mathbf{v}^{(m+1)} - \mathbf{v} \in W(\tilde{W})$ then by substitution of $\boldsymbol{\alpha}$ by $\mathbf{v}^{(m+1)} - \mathbf{v}$ in equations (13) and (14) and by subtraction one obtains

$$\mu((\mathbf{v}^{(m+1)} - \mathbf{v}, \mathbf{v}^{(m+1)} - \mathbf{v})) + i\omega\rho(\mathbf{v}^{(m+1)} - \mathbf{v}, \mathbf{v}^{(m+1)} - \mathbf{v}) = -(p^{(m)} - p, \operatorname{div}(\mathbf{v}^{(m+1)} - \mathbf{v})),$$

which can be written with the classical induced norms

$$\mu \| \mathbf{v}^{(m+1)} - \mathbf{v} \|^2 + i\omega\rho |\mathbf{v}^{(m+1)} - \mathbf{v}|^2 = -(p^{(m)} - p, \operatorname{div}(\mathbf{v}^{(m+1)} - \mathbf{v})). \tag{16}$$

Using (15) with $q = q^{(m+1)} = p^{(m+1)} - p$, and $(q, \operatorname{div} \mathbf{v}^{(m+1)}) = (q, \operatorname{div}(\mathbf{v}^{(m+1)} - \mathbf{v})) \forall q \in Q(\tilde{Q})$ one obtains

$$(q^{(m+1)} - q^{(m)}, q^{(m+1)}) - C(\operatorname{div}(\mathbf{v}^{(m+1)} - \mathbf{v}), q^{(m+1)}) = 0. \tag{17}$$

(16) becomes

$$\mu \| \mathbf{v}^{(m+1)} - \mathbf{v} \|^2 + i\omega\rho |\mathbf{v}^{(m+1)} - \mathbf{v}|^2 = -(q^{(m)}, \operatorname{div}(\mathbf{v}^{(m+1)} - \mathbf{v})). \tag{18}$$

But (17) can also be written:

$$2C\operatorname{Re}(\operatorname{div}(\mathbf{v}^{(m+1)} - \mathbf{v}), q^{(m+1)}) = |q^{(m+1)}|^2 - |q^{(m)}|^2 + |q^{(m+1)} - q^{(m)}|^2,$$

where Re denotes the real part.
With (18) one obtains

$$-2C\operatorname{Re}(\operatorname{div}(\mathbf{v}^{(m+1)} - \mathbf{v}), q^{(m)}) = 2C\mu \| \mathbf{v}^{(m+1)} - \mathbf{v} \|^2$$

and consequently

$$|q^{(m+1)}|^2 - |q^{(m)}|^2 + |q^{(m+1)} - q^{(m)}|^2 + 2\mu C \| \mathbf{v}^{(m+1)} - \mathbf{v} \|^2 = 2C\operatorname{Re}(\operatorname{div}(\mathbf{v}^{(m+1)} - \mathbf{v}), q^{(m+1)} - q^{(m)}). \tag{19}$$

But

$$|2C(\operatorname{div}(\mathbf{v}^{(m+1)} - \mathbf{v}), q^{(m+1)} - q^{(m)})|_{\mathbb{C}} \leqslant 2|C| |\operatorname{div}(\mathbf{v}^{(m+1)} - \mathbf{v})| |q^{(m+1)} - q^{(m)}|$$

and

$$\| \mathbf{v}^{(m+1)} - \mathbf{v} \|^2 = |\operatorname{div}(\mathbf{v}^{(m+1)} - \mathbf{v})|^2 + |\operatorname{rot}(\mathbf{v}^{(m+1)} - \mathbf{v})|^2.$$

Then

$$|2C\operatorname{Re}(\operatorname{div}(\mathbf{v}^{(m+1)} - \mathbf{v}), q^{(m+1)} - q^{(m)})| \leqslant 2|C| \| \mathbf{v}^{(m+1)} - \mathbf{v} \| |q^{(m+1)} - q^{(m)}|. \tag{20}$$

Let $C \in \mathbb{R}^+$, $\delta \in \mathbb{R}$, $0 < \delta < 1$

Then

$$2C \| \mathbf{v}^{(m+1)} - \mathbf{v} \| |q^{(m+1)} - q^{(m)}| \leqslant \delta |q^{(m+1)} - q^{(m)}|^2 + \frac{C^2}{\delta} \| \mathbf{v}^{(m+1)} - \mathbf{v} \|^2. \tag{21}$$

And in using (21), (20) and (19) one obtains

$$|q^{(m+1)}|^2 - |q^{(m)}|^2 + |q^{(m+1)} - q^{(m)}|^2 + 2\mu C \| \mathbf{v}^{(m+1)} - \mathbf{v} \|^2 \leqslant \delta |q^{(m+1)} - q^{(m)}|^2 + \frac{C^2}{\delta} \| \mathbf{v}^{(m+1)} - \mathbf{v} \|^2$$

or, in another form,

$$|q^{(m+1)}|^2 - |q^{(m)}|^2 + (1-\delta)|q^{(m+1)} - q^{(m)}|^2 + C\left(2\mu - \frac{C}{\delta}\right) \| \mathbf{v}^{(m+1)} - \mathbf{v} \|^2 \leqslant 0.$$

By adding up the previous inequality from $m = 0$ to N, one obtains:

$$|q^{(N+1)}|^2 + (1-\delta) \sum_{m=0}^{N} |q^{(m+1)} - q^{(m)}|^2 + C\left(2\mu - \frac{C}{\delta}\right) \sum_{m=0}^{N} \| \mathbf{v}^{(m+1)} - \mathbf{v} \|^2 \leqslant |q^{(0)}|^2.$$

Then necessarily

$$|q^{(m+1)} - q^{(m)}|^2 = |p^{(m+1)} - p^{(m)}|^2 \to 0 \quad \text{when} \quad m \to \infty, \quad \| \mathbf{v}^{(m+1)} - \mathbf{v} \|^2 \to 0 \quad \text{when} \quad m \to \infty,$$

If $C(2\mu - (C/\delta)) > 0$, $0 < (C/2\mu) < \delta < 1$.

In conclusion, the convergence of the velocity is demonstrated. But the corresponding result for the pressure is weaker (as for the classical Stokes problem).

NUMERICAL IMPLEMENTATION AND TESTS

Numerical implementation

The linear system of equations, associated with equation (15), of the Uzawa algorithm is easy to solve. In fact the problem is solved on each element separately.

The pressure is discontinuous from one element to another; then it is not necessary to assemble the elements. Moreover, in this equation (15), the imaginary part and the real part are not coupled.

But for the linear system of equations, associated with equation (14) of the Uzawa algorithm, elements are linked together. Then to build and solve this linear system of equations we have used a frontal method.[9] This technique was developed in Grenoble by Aussems[10] for symmetrical problems, and by Chambon[6] and Poncet[11] for non-symmetrical problems in solid mechanics. Naturally in (14) the dynamical term $(i\omega\rho(\mathbf{v}^{(m+1)}, \boldsymbol{\alpha}))$ induces a coupling between the imaginary part and the real one of the unknown functions. Then with six nodes on each element, it gives 24 degrees of freedom on each triangle. Moreover it is easy to see that the linear system can be written

$$\begin{bmatrix} [\mathbf{A}] & -\omega[\mathbf{B}] \\ \omega[\mathbf{B}] & [\mathbf{A}] \end{bmatrix} \begin{Bmatrix} \mathrm{Re}\{\mathbf{v}_N\} \\ \mathrm{Im}\{\mathbf{v}_N\} \end{Bmatrix} = \begin{Bmatrix} \mathrm{Re}\{\mathbf{C}\} \\ \mathrm{Im}\{\mathbf{C}\} \end{Bmatrix}, \tag{22}$$

where $[\mathbf{A}]$ and $[\mathbf{B}]$ are symmetrical matrices with real components; $\mathrm{Re}\{\mathbf{v}_N\}$ and $\mathrm{Im}\{\mathbf{v}_N\}$ are, respectively, the real and imaginary parts of the velocity nodal unknown functions; $\mathrm{Re}\{\mathbf{C}\}$ and $\mathrm{Im}\{\mathbf{C}\}$ are the real and imaginary parts of the right hand side term of equation (14); ω is the pulsation.

Let us note that the matrix of the system is more and more non-symmetric when frequency is increasing. The tests hereafter illustrate this remark.

The triangular elements are built using an automatic process. Quadrilateral elements are given by the equipotential lines and the flow lines of the hydrodynamical flow in the same media. These lines are computed using conformal transformations[12] and then, by division, triangular elements as 'regular' as possible are obtained.

Finally, particular boundary conditions such as Ω-periodicity need some explanations. The homogeneous boundary conditions on Γ_1 are classical. They are treated by a penalization method. In fact the numerical implementation of periodicity is very simple; the frontal method is well-adapted.

First we assume spacial periodicity for the $2n$ nodes on Γ_2, as is shown in Figure 5.

The Ω-periodicity of unknown functions is assumed by numerical identification of the nodes A_i and B_i. For the computer, the A_i node number would be the same as the B_i node number ($i = 1$ to N). Then, when elements are assembled, no difference is done between A_i and B_i. For instance, let us consider a narrow slit (Figure 6). The equivalent numerical picture is shown in Figure 7. This is the same as a doubly connected set.

In conclusion, let us notice that for many steps of Uzawa algorithm, only the second member of (22) is changed. Then the construction and the triangulation of the matrix

$$\begin{bmatrix} [\mathbf{A}] & -\omega[\mathbf{B}] \\ \omega[\mathbf{B}] & [\mathbf{A}] \end{bmatrix}$$

is only performed during the first step

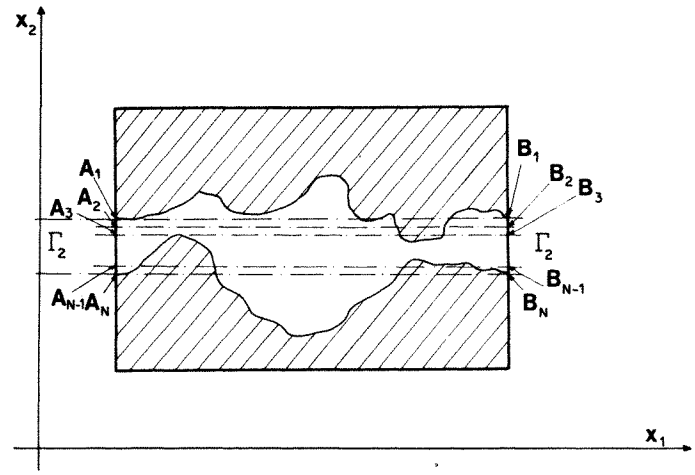

Figure 5. The periodicity of the nodes on Γ_2. For $i = 1$ to N; $x_2(A_i) = x_2(B_i)$

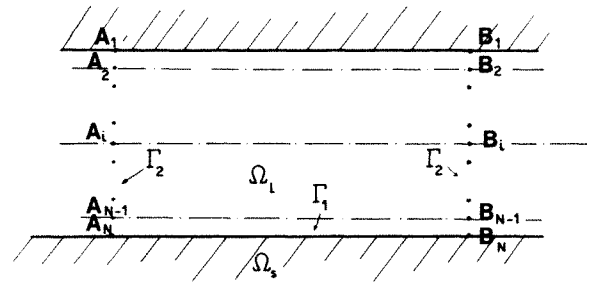

Figure 6. The boundary condition on Γ_2 in the case of a narrow slit

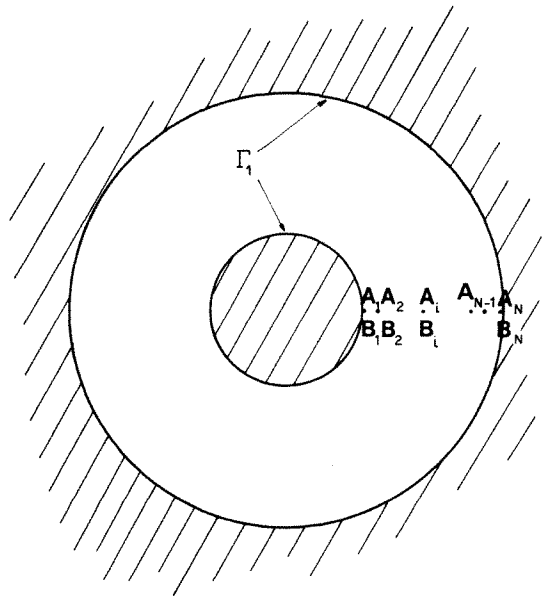

Figure 7. The equivalent numerical picture of the narrow slit

Tests

It is convenient to test the efficiency of the method on an example where the analytical solution is known. As is shown by Avallet[13] for the narrow slit (Figure 8) the analytical solution for the velocity is

$$v_1 = \frac{F}{i\omega\rho}\left[1 - \frac{\cosh\left[x_2\sqrt{\left(\frac{i\omega}{\nu}\right)}\right]}{\cosh\left[a\sqrt{\left(\frac{i\omega}{\nu}\right)}\right]}\right] \quad (\omega \neq 0),$$

$$v_1 = a^2 - x_2^2 \quad (\omega = 0),$$

where ω is the pulsation, p is the fluid density, F is the macroscopic pressure gradient and $\nu = \rho\mu$ with μ the dynamical viscosity.

Then many parameters are tested and, in particular,

(i) refinement in the mèsh
(ii) the efficiency of the bulb function
(iii) the constant C and the convergence of the Uzawa algorithm
(iv) the convergence of the Uzawa algorithm when the frequency is increasing
(v) the part of the initial pressure distribution.

First, let us define an error parameter at the step m of the Uzawa algorithm. Let $V_i^{(m)}(i = 1, 2)$ be a component of the average complex velocity on Ω_f^d at the step m.

$$V_i^{(m)} = \frac{1}{|\Omega|}\int_{\Omega_f^d} v_i^{(m)}(M)\mathrm{d}\Omega$$

The numerical problem is solved in a non-dimensional form. In the following the subscript (a) in parentheses denotes non-dimensional quantities. Let us define these non-dimensional quantities. If a is a typical dimension of the pores Ω_f^d, ρ is the fluid mass per unit of fluid volume and μ is the dynamic viscosity ($\nu = \mu/\rho$), the different non-dimensional quantities can be taken as:

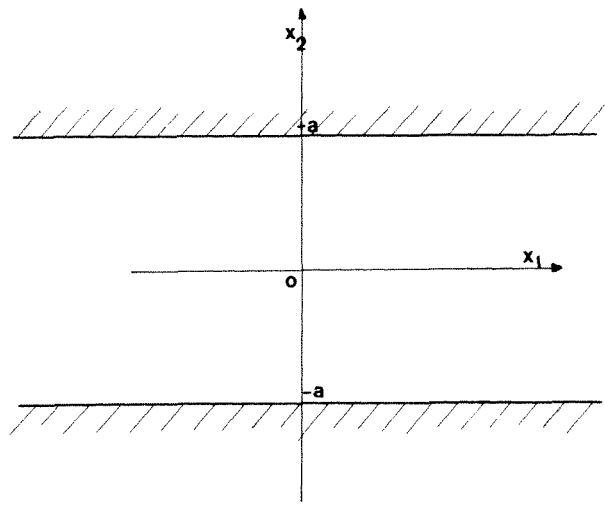

Figure 8. A narrow slit

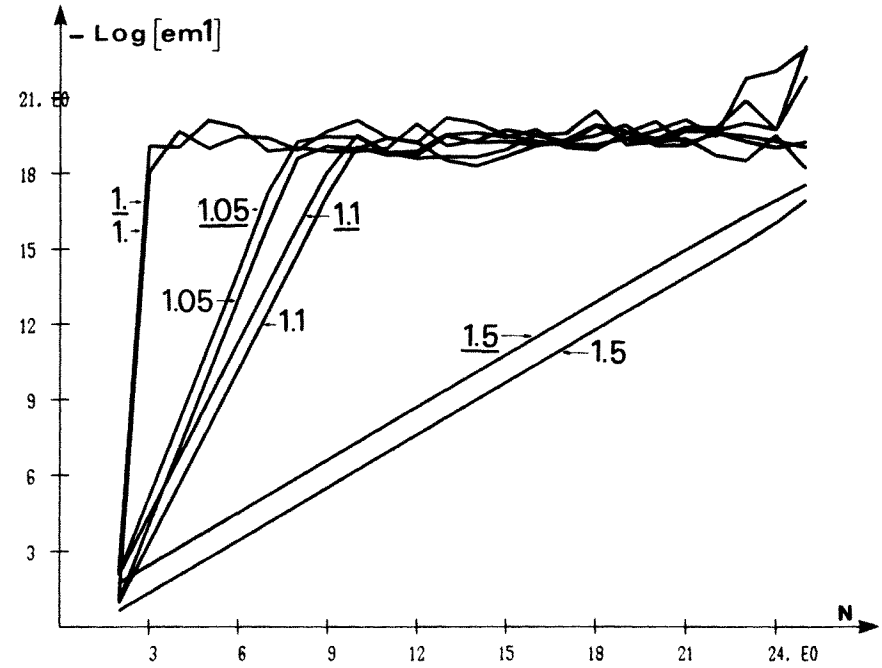

Figure 9. Log(em1) against the number of iteration N with $\omega_{(a)} = 0$ and for several values of C. The underlined values of C denote computations with bulb function. (Figure 16(a) gives the mesh which is used)

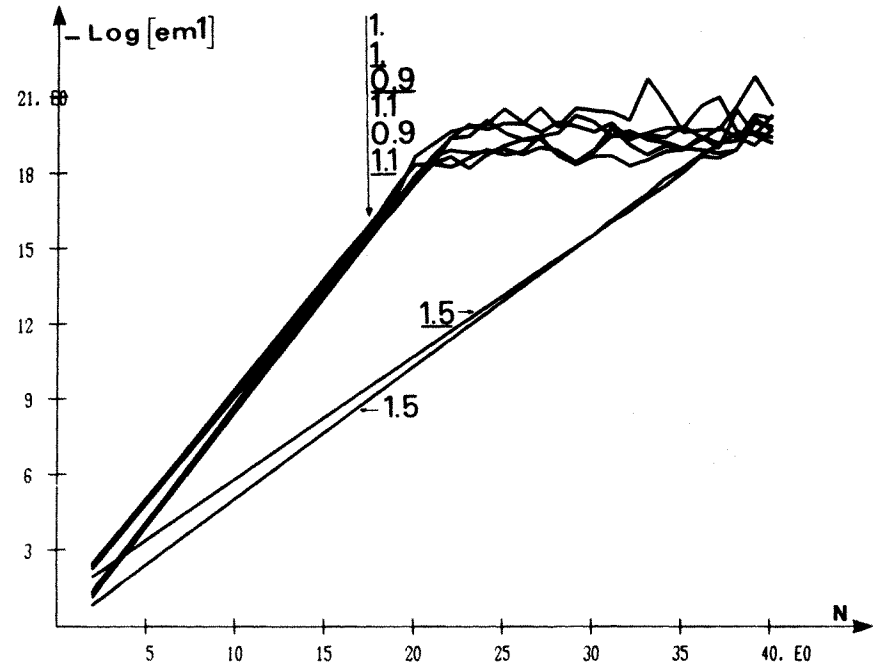

Figure 10. Same as Figure 9 with $\omega_{(a)} = 1$

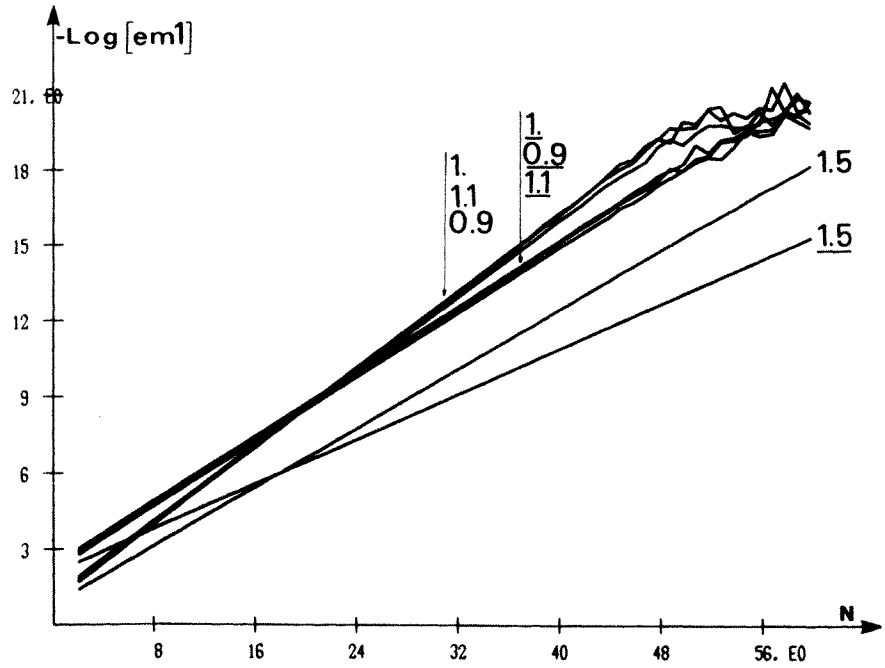

Figure 11. Same as Figure 9 with $\omega_{(a)} = 2{\cdot}32$

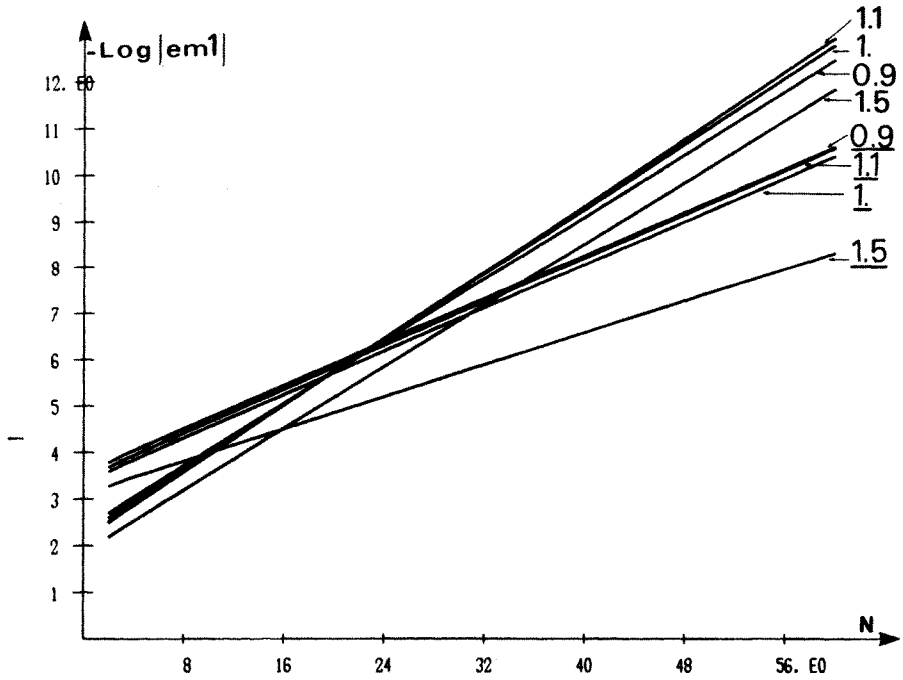

Figure 12. Same as Figure 9 with $\omega_{(a)} = 4{\cdot}25$

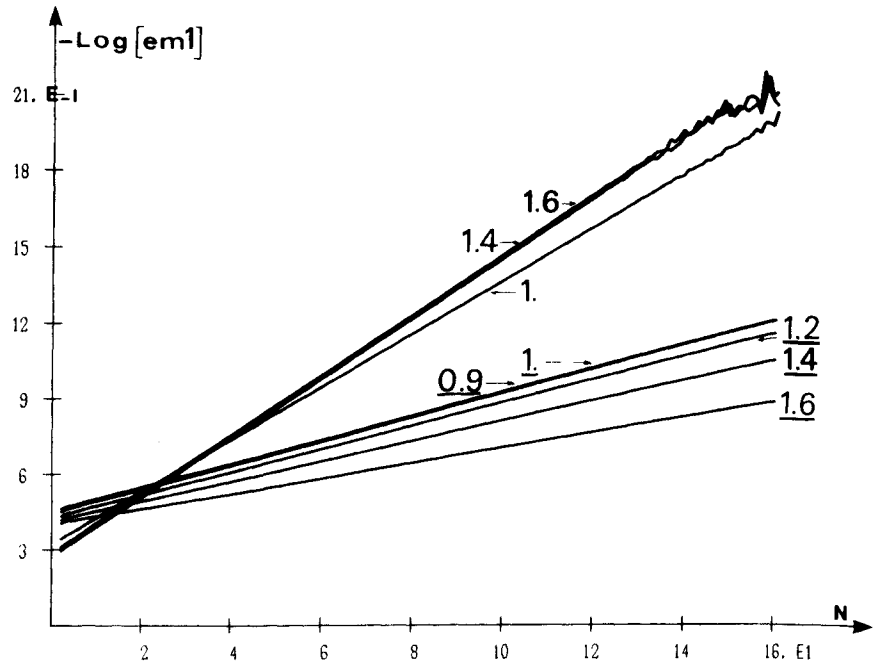

Figure 13. Same as Figure 9 with $\omega_{(a)} = 7$

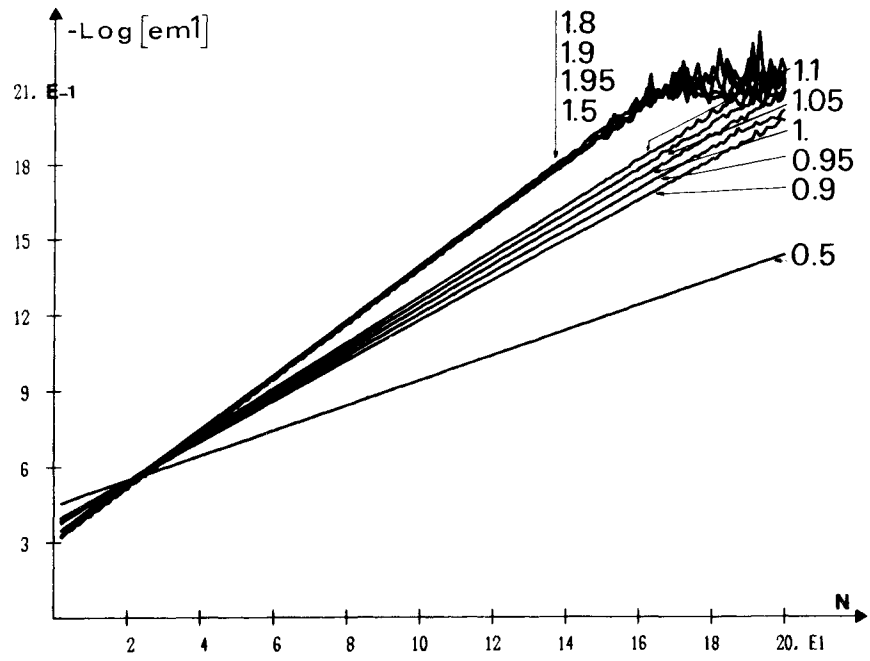

Figure 14. Same as Figure 9 with $\omega_{(a)} = 9$

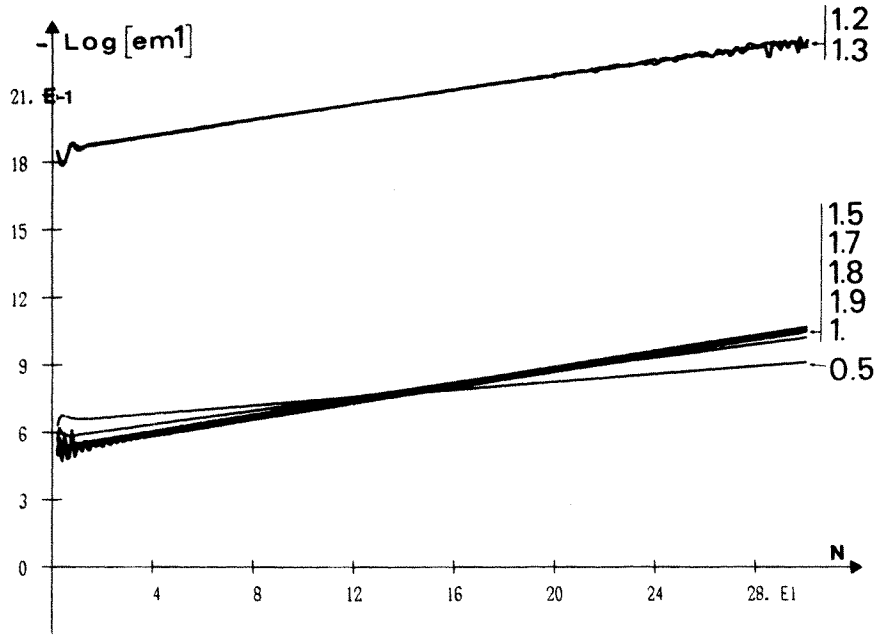

Figure 15. Same as Figure 9 with $\omega_{(a)} = 20$, but for a different mesh (Figure 16(b))

For the pulsation ω:

$$\omega_{(a)} = \frac{\omega a^2}{2\nu},$$

the velocity $\mathbf{v}$:

$$\mathbf{v}_{(a)} = \frac{a\mathbf{v}}{\nu},$$

the (microscopic) pressure p:

$$p_{(a)} = \frac{a^2 p}{\nu\mu},$$

the macroscopic pressure gradient $\mathbf{F}$:

$$\mathbf{F}_{(a)} = \frac{a^3 \mathbf{F}}{2\mu\nu},$$

the spatial variable x_i:

$$x_{i(a)} = \frac{x_i}{a}.$$

$$V_{i(a)}^{(m)} = \frac{1}{|\Omega|} \int_{\Omega_f^d} v_{i(a)}^{(m)} \mathrm{d}\Omega$$

The error parameter $\mathrm{em}1^{(m)}$ is defined by

$$\mathrm{em}1^{(m)} = \frac{1}{4}\sqrt{\left[\sum_{i=1}^{2}\left(|V_{i(a)}^{(m)}|^2 - |V_{i(a)}^{(m-1)}|^2\right)\right]}.$$

Figures 9–15 give $\mathrm{em}1^{(m)}$ for different values of $\omega_{(a)}$. In each Figure computations are performed with the same spatial discretization. The corresponding mesh is given in Figure 16. In each Figure, several kind of computations are performed: (a) for different values of the parameter C of Uzawa's algorithm, and (b) for the two discrete problems (with or without the bulb function). Note that on the Figures, computations with bulb function are represented by an underlined parameter C.

The set of all computations performed on this particular case leads to the following comments:

1. Refinement of the mesh gives similar numerical solution, as the two kinds of computations (with or without the bulb function). Nevertheless, a refinement in the mesh would be necessary for a

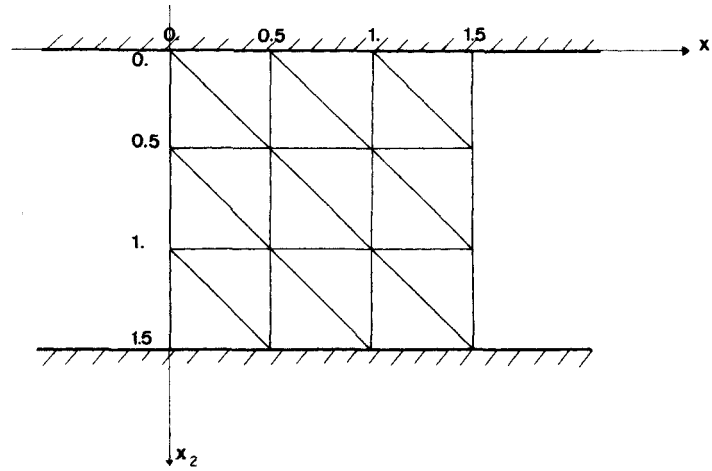

Figure 16(a) A mesh for the narrow slit

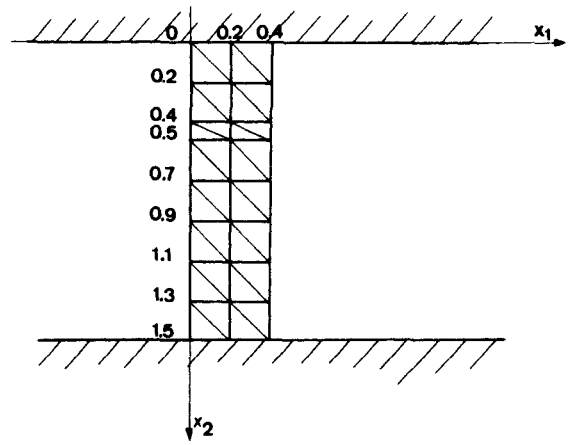

Figure 16(b) Refinement of the previous mesh

Table I. Optimum Parameter C for different pulsation $\omega_{(a)}$ and for the two kinds of computations (with or without bulb function), for mesh of figure 16.

$\omega_{(a)} = \frac{\omega a^2}{2\nu}$	0	1	2·32	4·25	7	9
$0 < C < 2$ without bulb function	1	1	1	1·1	1·4	1·8
$0 < C < 2$ with bulb Function	1	1	1	1	1	1

more complicated geometrical problem. This will be the case in the next section. The efficiency of the bulb function is difficult to evaluate for the narrow slit. Let us notice that for $\omega = 0$, the quadratic interpolation for the velocity gives the analytical solution, as for the pressure which is uniform.

2. The best value for the parameter C and the convergence of the Uzawa algorithm is a function of the non-dimensional pulsation ω and the kind of computation (with or without the bulb function). The results are summarized in Table I.

3. For 'high' frequencies, convergence of the Uzawa algorithm is weak. Then the computations (with or without the bulb function) becomes expensive and less and less accurate. This is an important restriction for these computations. This behaviour is explained by the structure of the matrix of the linear system (22):

$$\begin{bmatrix} [\mathbf{A}] & -\omega[\mathbf{B}] \\ \omega[\mathbf{B}] & [\mathbf{A}] \end{bmatrix}.$$

This matrix becomes more and more non-symmetric when the frequency is increasing.

4. The initial pressure distribution does not take any part in the velocity of convergence of the Uzawa algorithm (see Figure 15 for $C = 1{\cdot}2$ and $C = 1{\cdot}3$).

NUMERICAL EXPERIMENT

In order to compute the components $K_{11}(\omega)$ of the generalized permeability tensor $\mathbf{K}(\omega)$ for the new geometry sketched in Figure 17 several computations are performed:

(a) with or without the bulb function

(b) for two different meshes: mesh A (Figure 18) and mesh B (Figure 19).

In the following the component $K_{11}(\omega)$ will be denoted as $K(\omega)$. As previously, the results are presented in non-dimensional form.

Let us define

$$H(\omega) = \frac{1}{K(\omega)} = H1(\omega) + \mathrm{i}H2(\omega)$$

and n, the porosity of the media,

$$n = \frac{|\Omega_f|}{|\Omega|}$$

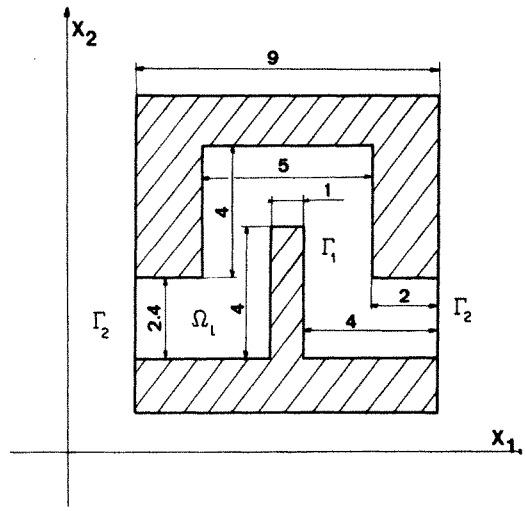

Figure 17. Another geometrical period Ω to study

The viscous dissipation $H1(\omega)$

$$H1_{(a)}(\omega_{(a)}) = \frac{na^2 H1(\omega)}{2\mu}$$

The inertial part $H2(\omega)$

$$H2_{(a)}(\omega_{(a)}) = \frac{nH2(\omega)}{\rho\omega}$$

and

$$|H_{(a)}(\omega_{(a)}) = \frac{na^2|H(\omega)|}{2\mu}$$

$$\tan\varphi = \frac{H2(\omega)}{H1(\omega)}$$

To test the dynamic behaviour of the media, the results of computations are compared to those of a narrow slit, which is defined by the following 'equivalence property'.

The two media (Figure 17 and the narrow slit) are said to be 'equivalent' if they have the same static permeability $K(\omega = 0)$ and the same porosity. Let us note that for any media, with the scale parameter a, an 'equivalent' narrow slit can be found.

In Figures 20 and 21 the numerical results are compared with an 'equivalent' narrow slit.

In Figures 22 and 23 the same numerical results are compared to the experimental data.

The set of these computational results leads to new comments. The previous conclusions for the narrow slit are still valid.

For the computations without the bulb function and for the two meshes the results are different. A refinement in the mesh gives a best numerical solution but a great number of degrees of freedom is rapidly reached. Another refinement in the mesh to test the validity of solution of the mesh B has not be performed. It would be too expensive in C.P.U. time and in memory. The computations on mesh B lead to about 5500 degrees of freedom. This is an important limitation for computations.

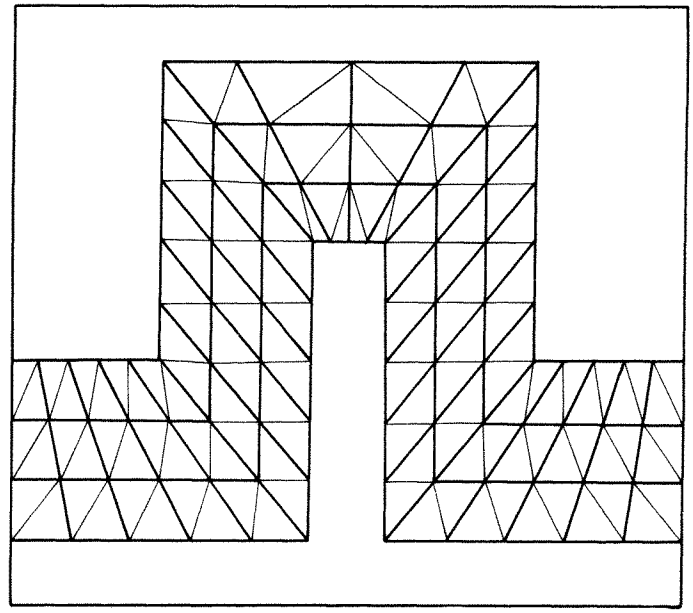

Figure 18. A first mesh (A) for our problem

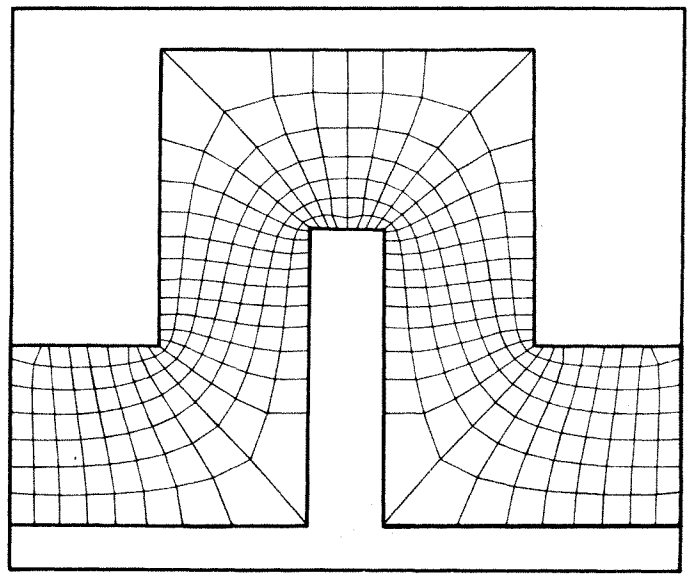

Figure 19. A second mesh (B) for our problem. Quadrilateral elements are divided into two triangles by the shortest diagonal.

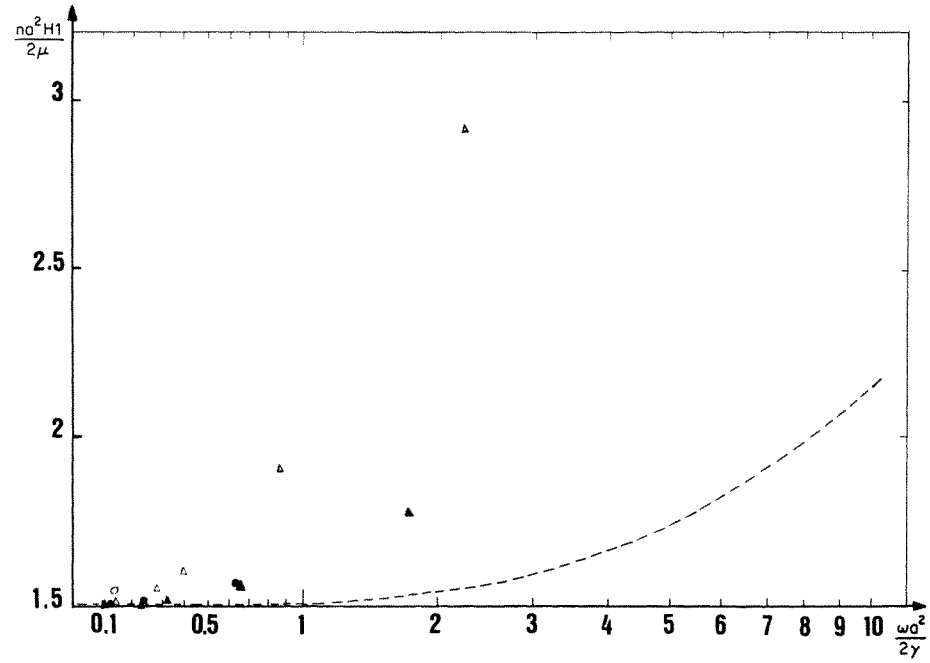

Figure 20. $H1_{(a)}$ against frequency $\omega_{(a)}$:----the equivalent narrow slit. Numerical results: △ mesh A without bulb function; ▲ mesh A with bulb function; ○ mesh B without bulb function; ● mesh B with bulb function

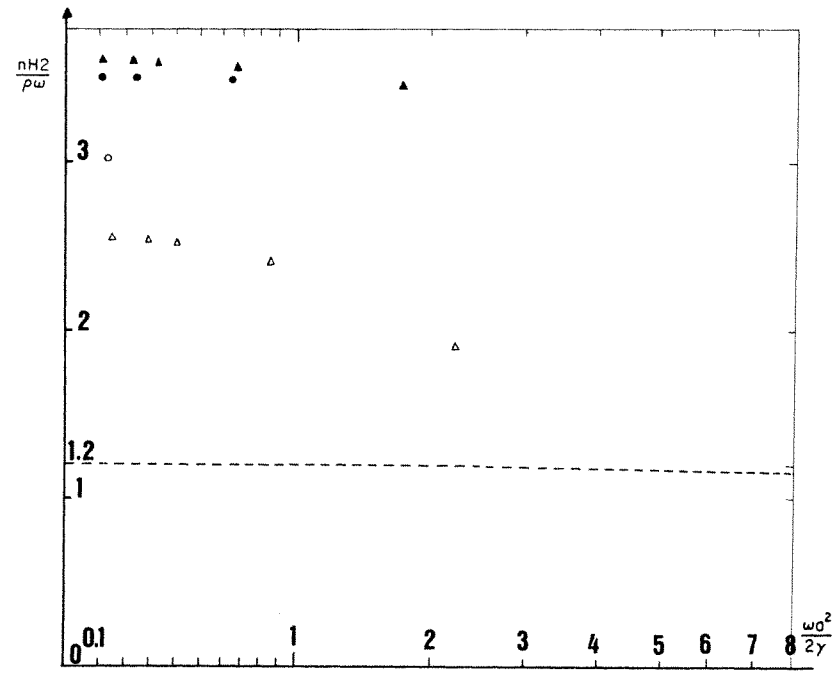

Figure 21. $H2_{(a)}$ against frequency $\omega_{(a)}$. Notations as in Figure 20

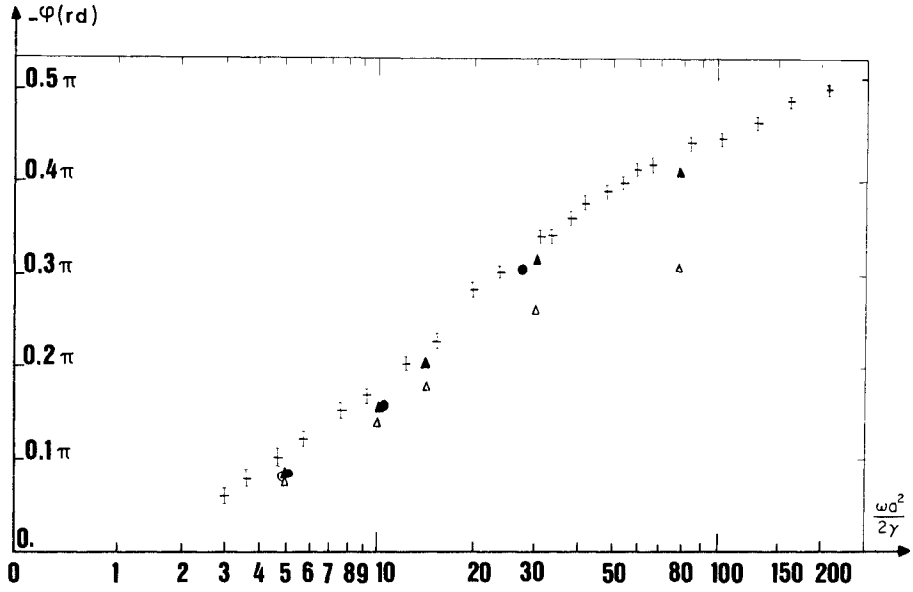

Figure 22. Phase against frequency $\omega_{(a)}$: I experimental data; numerical results: as in Figure 20

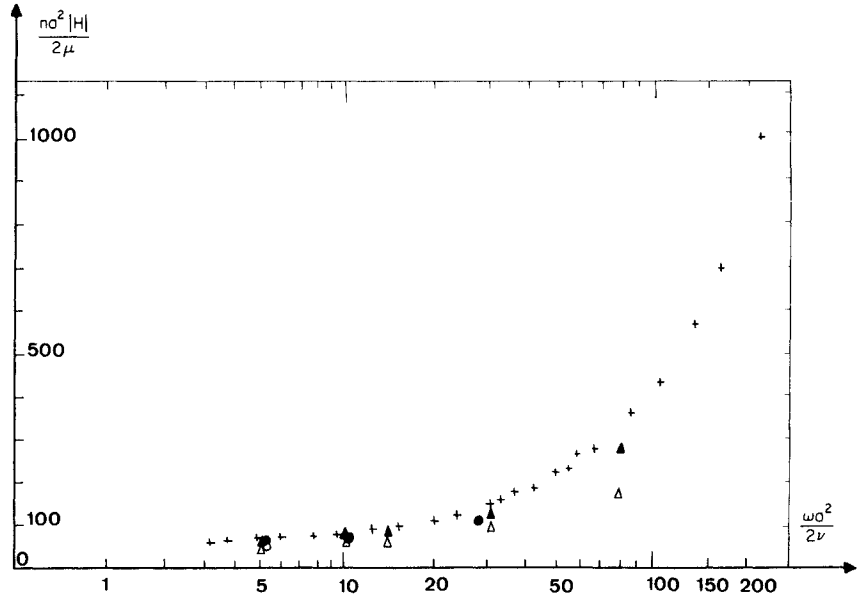

Figure 23. $|H_{(a)}|$ against frequency $\omega_{(a)}$: + experimental data; numerical results: as in Figure 20

A refinement in the shape functions (bulb function) provides better results. The computations with the bulb function for the two meshes A and B are in agreement. The cost of such a refinement is very low. It does not add many degrees of freedom. Moreover the supplementary node is an interior one, which is treated on the element. The dimension of the linear system to be solved is not changed.

CONCLUSION

In conclusion, the extension to complex unknown functions of the methods of Crouzeix and Raviart[8] gives good results. The interest of the bulb function seems to be obvious. Nevertheless two important limitations of these computations are demonstrated. Conforming elements of Crouzeix and Raviart provide a big linear system. The use of non-conformal finite element could perhaps reduce the dimension of the problem, without loss in precision. The computations for 'high' frequencies are difficult and expensive. A refinement in the algorithm would be tested.

REFERENCES

1. J. L. Auriault, 'Dynamic behavior of a porous media saturated by a newtonian fluid', *Int. J. Enging. Sci*, **18,** 775–785 (1980).
2. J. L. Auriault, 'Homogenization-application to porous saturated media', Summer school, Gdansk, September 1983.
3. J. L. Auriault and E. Sanchez-Palencia, 'Etude du comportement macroscopique d'un milieu poreux saturé déformable', *J. de Mécanique*, **16,** (4) 575–603 (1977).
4. J. L. Auriault, L. Borne and R. Chambon, 'Dynamics of porous saturated media, checking of the generalized law of Darcy' *J. Acoust. Soc. Am.* **77,** (5) 1641–1650 (1985).
5. L. Borne, 'Contribution à l'étude du comportement dynamique des milieux poreux saturés déformables', *Thèse Doc. Ingenieur*, Grenoble, 1983.
6. R. Chambon, F. Darve and G. Tratapel, 'Mesures et calculs avec loi non-lineaire pour un modèle expérimental', *Symposium Franco-Polonais. Problèmes non-lineaires de mécanique*, Cracovie, 1977.
7. R. Temam, 'Navier–Stokes *Equations*, North Holland, Amsterdam, 1977.
8. M. Crouzeix and P. A. Raviart, 'Conforming and non-conforming finite element methods for solving the stationary Stokes equations', *R.A.I.R.O., Analyse numérique*, **3,** 33–76 (1973).
9. B. Irons, 'A frontal solution program for finite element analysis', *Int. j. numer. methods eng.*, **2** (1970).
10. A. Aussems, 'Une mise en oeuvre frontale des méthodes d'élements finis', *Thèse Doc-Ing*, Grenoble, 1972.
11. A. Poncet, 'Autour de l'écriture d'un code d'éléments finis', *Thèse d'état*, Grenoble, 1979.
12. R. Chambon, 'Application de la méthode des éléments finis et d'une loi rhéologique incrémentale aux calculs de mécanique des sols', *Thèse Doc-Ing*, Grenoble, 1975.
13. C. Avallet, 'Comportement dynamique de milieux poreux saturés déformables', *Thèse 3ème cycle*, Grenoble, 1981.
14. M. Bercovier and M. Engelman, 'A finite element for the numerical solution of viscous incompressible flow', *J. Comp. Phys*, **30,** 180–201 (1980).
15. M. Fortin and M. Soulie 'A non-conforming piecewise quadratic finite element on triangles', *Int. j. numer. methods eng.*, **19,** 505–520 (1983).
16. T. J. R. Hughes, W. K. Liu and A. Brooks, 'Finite element analysis of incompressible viscous flows by the penalty function formulation', *J. Comp. Phys*, **30,** 1–60 (1979).
17. P. A. Raviart, 'Les méthodes d'eléments finis en mécanique des fluides', *C.E.A.—E.D.F.—I.N.R.I.A.—Ecole d'été d'analysis numérique*, Collection de la direction des études et recherches d'Electricité de France, Eyrolles.
18. O. C. Zienkiewicz, '*La Méthode des Éléments finis*, Edisciences.